MAGNETIC RESONANCE IN MEDICINE 25, 390–397 (1992)

Time Course EPI of Human Brain Function during Task Activation

PETER A. BANDETTINI,* ERIC C. WONG,* R. SCOTT HINKS,†
RONALD S. TIKOFSKY,* AND JAMES S. HYDE*

** Department of Radiology, Medical College of Wisconsin, Milwaukee, Wisconsin 53226; and † Applied Science Laboratory, GE Medical Systems, Waukesha, Wisconsin 53288*

Received February 5, 1992; revised March 31, 1992; accepted March 31, 1992

Using gradient-echo echo-planar MRI, a local signal increase of 4.3 ± 0.3% is observed in the human brain during task activation, suggesting a local decrease in blood deoxyhemoglobin concentration and an increase in blood oxygenation. Images highlighting areas of signal enhancement temporally correlated to the task are created.

INTRODUCTION

Blood is a unique source of physiological contrast in MRI due to its oxygenation-sensitive paramagnetic characteristics. Deoxyhemoglobin contains paramagnetic iron, while oxyhemoglobin contains diamagnetic oxygen-bound iron (*1*). The partial pressure of oxygen in blood regulates the oxygen saturation of hemoglobin, as described empirically by the oxygen–hemoglobin dissociation curve (*2*).

It is well established that the oxygen saturation of hemoglobin affects the T_2 of whole blood (*1, 3–8*). An explanation for this effect has been proposed (*1*). The susceptibility differential between the hemoglobin-containing erythrocyte and surrounding plasma creates microscopic field inhomogeneities. Irreversible dephasing is caused by exchange of protons across the erythrocyte membrane and/or diffusion of protons through the microscopic magnetic field gradients.

On a larger scale, it has been demonstrated that the paramagnetic contribution of deoxyhemoglobin affects the susceptibility of whole blood (*9–11*), causing it to be less diamagnetic than surrounding tissue. Magnetic field inhomogeneities within and around each vessel are created by this susceptibility differential (*12*). A spin-echo is attenuated by dephasing due to diffusion of spins through field inhomogeneities (*13, 14*), while a gradient-echo is additionally attenuated by dephasing due to static field inhomogeneities, independent of diffusion (*9, 10, 15–17*).

Recent work demonstrates the sensitivity of gradient-echo imaging to oxygenation changes in both larger vessels and capillaries. Ogawa *et al.* (*9, 10*) demonstrate oxygenation-sensitive contrast in rodent cerebral vessels using a gradient-echo imaging sequence at 7 T. Turner *et al.* (*16, 17*), observe, at 2 T, oxygenation-dependent T_2^* changes in the cat brain attributed to increases in the concentration of deoxyhemoglobin in cerebral veins and capillaries. The changes in T_2^* are observed through the time course collection of images obtained with a long-TE echo-planar imaging (EPI) sequence which samples during the free induction decay. This sequence is referred to

0740-3194/92 $5.00

as gradient-echo EPI. A long TE enhances the effects of a susceptibility differential by allowing more time for spin dephasing to occur within a voxel.

Using long-TE gradient-echo EPI without administered contrast agents, preliminary success in brain activity imaging has been reported. Photic stimulation-induced signal change in the human brain has been reported by Brady (*18*). Task activation-induced signal change in the human brain has been reported by Bandettini *et al.* (*19*).

We demonstrate that time course, long-TE, gradient-echo EPI is an effective tool in localizing brain function in humans. Signal increases that occur during task activation are observed to be predominantly in the primary motor and sensory areas functionally associated with the task (*2, 20*). Images are created in which these regions of temporally correlated signal enhancement are highlighted.

EQUIPMENT AND METHODS

All imaging was performed on a standard clinical GE 1.5-T Signa system using local gradient coils designed for rapid gradient switching. A 26.5-cm-i.d. three-axis head gradient coil, designed by E. C. Wong, and a prototype GE 33.0-cm-i.d. z-axis head gradient coil were used. A blipped, gradient-echo EPI pulse sequence, having an initial $\pi/2$ pulse and an effective TE ($(k_x, k_y) = (0, 0)$) of 50 ms, was employed. The acquisition time was 40 ms for each 64 $\times$ 64 image, and was centered at the effective TE. All displayed images were linearly interpolated to a 256 $\times$ 256 matrix. A time course series of up to 128 sequential images of the same plane was obtained using an interscan delay or TR of 2 to 3 s. Slice thickness was 25 mm to ensure that the activated region of the brain was completely contained in the slice. The head of the subject was immobilized by tightly packed foam rubber cushions.

Each time course series was divided in time into three segments. During the first and last segments, the subject was instructed to remain completely relaxed. During the middle segment, the subject was instructed to touch each finger to thumb in a sequential, self-paced, and repetitive manner. Two experiments are presented. The first experiment observed local signal enhancement correlated with finger movement on the right hand and the second experiment observed local signal enhancement correlated with finger movement on both hands.

Synthesis of Brain Activity Images

All postprocessing was performed on a Sun SPARCstation 1+. Minor amounts of linear signal drift that occurred through the time course were removed using a baseline correction which was linear with respect to time. Brain activity images were obtained by calculating the correlation between the time response of each voxel and an ideal response to the task activation (*21*). If a time sequence of n images is obtained, each voxel is described by an n dimensional vector, here termed the voxel vector, whose components are the voxel values at each time point. An n dimensional ideal response vector is constructed by setting those components that occur during task activation to 1 and all other components to -1. The vector products of the ideal response vector with the voxel vectors are displayed in an image array, termed the brain activity image. The voxel values that increase in a manner temporally correlated to the finger movement activity have the highest values in the brain activity image.

Activated regions were located by reference to the brain activity images. Plots of signal from activated regions versus sequential image number were then made from the baseline drift-corrected images.

RESULTS

In the first experiment, 128 sequential coronal images (TR = 2 s) were acquired of a slice that covered a region of the primary sensory and motor areas of the subject (*2, 20*) using the 33.0-cm-i.d. *z*-axis gradient coil. The FOV was 24 cm, giving an in-plane resolution of 3.75 mm. During the acquisition of images 44 to 88, the subject was instructed to move the fingers on the right hand in the manner described above.

In the second experiment, a series of 72 sequential axial images (TR = 3 s) were acquired of a slice covering the entire superior region of the brain using the 26.5-cm-i.d. three-axis gradient coil. The FOV was 20 cm, giving an in-plane resolution of 3.12 mm. During the acquisition of images 25 to 51, the subject was instructed to move the fingers on both hands in the manner described above.

Figures 1a and 1b are the brain activity images obtained from the first and second experiments, respectively. The brightest regions in the images are areas of enhanced signal during task activation. The bright region at the base of the brain in Fig. 1a may be an artifact caused by the fact that the signal enhancement due to pulsatility of blood or cerebral spinal fluid flow in the neck and the scan repetition rate are of similar frequencies. A beat frequency between the two may have occurred during activation. This effect may bring into the functional images an artifact in the vicinity of pulsatile blood or cerebral spinal fluid flow.

Figures 2a and 2b are anatomical images from the first and second experiments, respectively. They are used here as anatomical references for the brain activity images. Threshold images of the brain activity images, created by setting the number of gray levels in Figs. 1a and 1b to two, were superimposed upon Figs. 2a and 2b, respectively. The brightest regions from the brain activity images correspond closely to areas of the cortex that are understood to be involved with finger activity (*2, 20*). These areas, known as the primary motor and sensory areas, are located on the precentral and postcentral gyri extending laterally from the midsagittal plane.

Figures 3 and 4 show plots of the signal intensity versus sequential image number from the regions of activation located by reference to the 64×64 brain activity images. The signal intensity values in Fig. 3 are mean values from the boxed 9-voxel region of activation in Fig. 1a. The boxed region is located along the central sulcus, contralateral to the right hand. The signal intensity values in Figs. 4a and 4b are the values of the boxed 1-voxel regions of activation in Fig. 1b. The regions in box 1 and box 2 are contralateral to the right and left hands, respectively. The observed signal intensity begins to increase and decrease within 3 s of finger movement initiation and cessation, respectively.

Procedures similar to the two described above were performed 24 times using six healthy volunteers. For each series of images, the values of the baseline-corrected signal from a 4-voxel area in the activated region were averaged across the resting-state images and the values of the baseline-corrected signal from the same 4-voxel area were averaged across the stimulated-state images. The difference between the two values was then divided by the average resting-state signal value to give the fractional

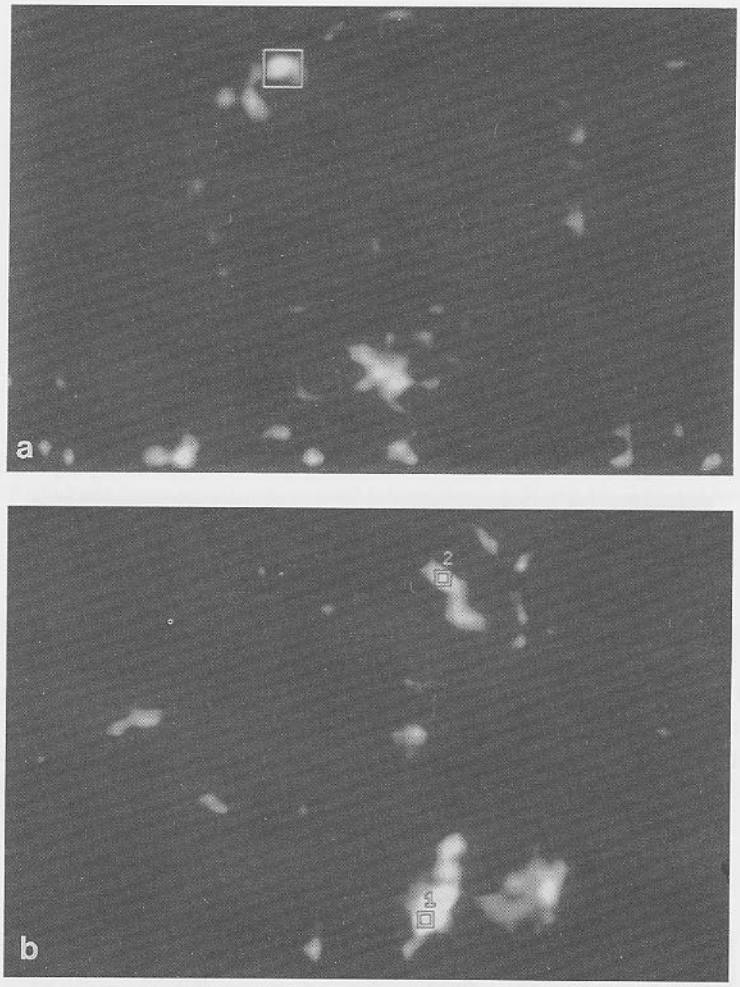

FIG. 1. Brain activity images. Brightest regions are areas of enhanced signal during the task of touching the fingers to the thumb in a repetitive, self-paced manner. Average signal intensities from boxed regions are plotted versus image number in Figs. 3 and 4. (a) Coronal brain activity image obtained from the first experiment in which the subject performed the task on the right hand. The slice contains the primary sensory and motor cortices. The brightest region in the cortex is in the hemisphere contralateral to the hand performing the task. (b) Axial brain activity image obtained from the second experiment in which the subject performed the task on both hands. Brightest regions appear to be in the primary sensory and motor cortices.

change corresponding to that experiment. All experimental results were then used to calculate the average fractional change in signal. The average signal increase observed in the activated regions during the finger movement task was $4.3 \pm 0.3\%$.

DISCUSSION

An increase in partial pressure of oxygen in the blood causes an increase in hemoglobin oxygen saturation, decreasing the concentration of deoxyhemoglobin (*3*).

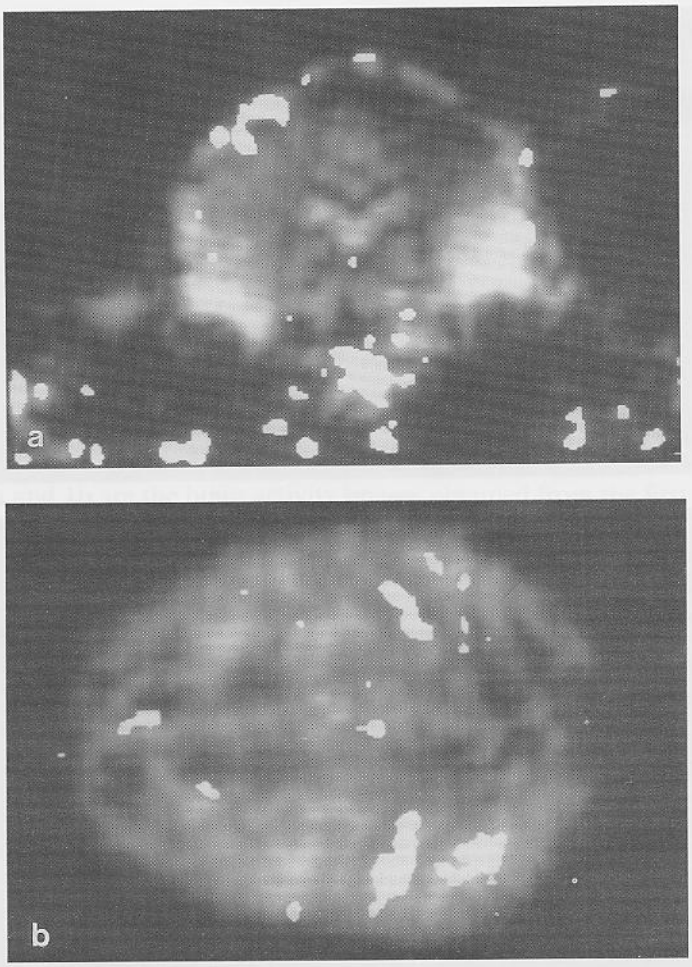

FIG. 2. Representative gradient-echo echo-planar images from each of the two series. TE = 50 ms. Slice thickness = 25 mm. Threshold images from the corresponding brain activity images are superimposed. (a) Coronal image from the 128-image series. A threshold image of Fig. 1a is superimposed. (b) Axial image from the 72-image series. A threshold image of Fig. 1b is superimposed.

It is postulated that the primary reason for the observed signal enhancement is the local decrease in the concentration of deoxyhemoglobin. A decrease in deoxyhemoglobin concentration decreases the tissue–blood susceptibility differential, thus decreasing spin dephasing and increasing signal. The local increase in signal upon cerebral tissue activation therefore suggests an increase in the blood oxygen partial pressure.

A local increase in the oxygen delivery beyond the metabolic need of activated cerebral tissue has been demonstrated by Fox *et al.* (*21*) with the use of positron emission tomography (PET). In the study, ^{15}O-labeled water and oxygen were used to measure cerebral blood flow (CBF) and oxygen extraction fraction (OEF), respectively. Cerebral metabolic rate of oxygen ($CMRO_2$) was determined by the product

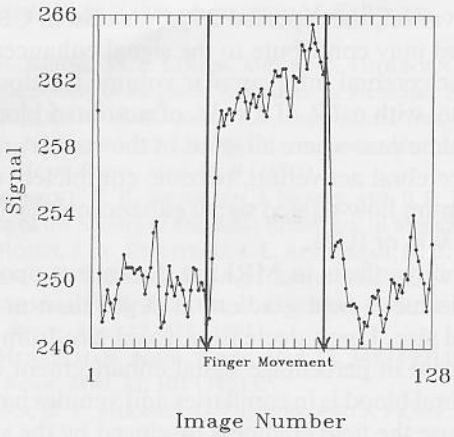

FIG. 3. Plot of signal intensity versus image number from the boxed 9-voxel region in Fig. 1a. Image spacing is 2 s. Right-hand finger movement occurred between images 44 and 88, indicated by the vertical arrows.

of OEF, CBF, and arterial oxygen content. During somatosensory stimulation, a 29% increase in CBF, a 5% increase in $CMRO_2$, and a 19% *decrease* in OEF were observed in the activated region, demonstrating a local uncoupling between CBF and $CMRO_2$. An overabundance of oxygen-rich blood is delivered to the activated region, causing the decrease in OEF. The decrease in OEF directly implies a local increase in the average blood oxygen partial pressure, which correlates qualitatively with the observed MR signal increase.

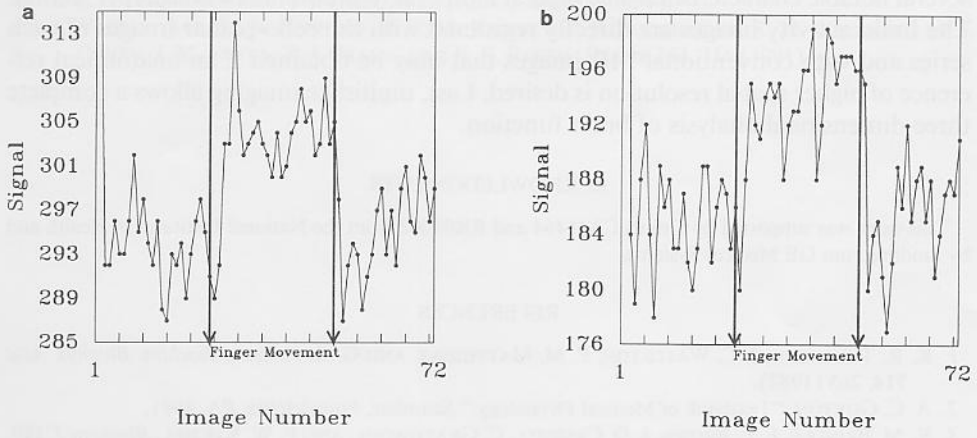

FIG. 4. Plots of signal intensity versus image number from the boxed 1-voxel regions in Fig. 1b. Image spacing is 3 s. Finger movement in both hands occurred between images 25 and 51, indicated by the vertical arrows. (a) Plot from box 1, contralateral to the right hand. (b) Plot from box 2, contralateral to the left hand.

During cerebral activation, the reported 29% increase in CBF increases the inflow of unsaturated spins and may contribute to the signal enhancement. The T_1 of blood is about 1 s (*4*), and the cerebral intravascular volume fraction is, at the most, about 4% (*23*). At steady state, with a TR of 2 s, M_z of saturated blood would equal $0.85 \times M_o$. Assuming the extreme case where all spins in the vessels are at steady state during rest and then, during cerebral activation, become completely unsaturated due to increased flow, the maximum flow-related signal enhancement would be approximately: $(1 - 0.85) \times 0.04 = 0.006$ or 0.6%.

In general, susceptibility effects in MRI are dependent upon voxel size when the scale of susceptibility-induced field gradient is larger than or on the same order of magnitude as the voxel size. Upon decreasing voxel size from 422 to 39.4 mm^3, we see no significant decrease in percentage signal enhancement during task activation. More than 70% of cerebral blood is in capillaries and venules having diameters ranging from 2 to 50 μm. Because the field gradients produced by the vessels generally extend to twice the vessel diameter (*9*), it is estimated that voxel size would have to be reduced to the range of 0.001 mm^3 to show a significant decrease in microvessel susceptibility-related intravoxel dephasing. Based on these estimates, the relative enhancement of signal observed in these experiments should be independent of voxel size within the range typically employed.

The imaging of regional circulatory, metabolic, and electrical phenomena that occur upon cerebral tissue stimulation has been achieved by many modalities (*24–27*). Among these modalities are electroencephalography, magnetoencephalography, PET, single photon emission computed tomography, and xenon computed tomography.

Recently, echo-planar MRI of dynamic susceptibility contrast induced by an intravenously administered paramagnetic contrast agent has proven to be an effective means of quantifying the increase in cerebral blood volume upon task activation (*28*).

Imaging human brain function using time course long-TE gradient-echo EPI, without the use of contrast agents, is now possible. The sequence presented in this study has several notable characteristics. The highest temporal resolution is 14 images per second. The brain activity images are directly registered with the echo-planar images of each series and with conventional MR images that may be obtained if an anatomical reference of higher spatial resolution is desired. Last, multislice imaging allows a complete three-dimensional analysis of brain function.

ACKNOWLEDGMENTS

This work was supported by Grants CA41464 and RR01008 from the National Institutes of Health and by funding from GE Medical Systems.

REFERENCES

1. K. R. Thulborn, J. C. Waterton, P. M. Matthiews, and G. K. Radda, *Biochim. Biophys. Acta* **714,** 265 (1982).
2. A. C. Guyton, "Textbook of Medical Physiology," Saunders, Philadelphia, PA, 1991.
3. K. M. Brindle, F. F. Brown, I. D. Campbel, C. Grathwohl, and P. W. Kuchel, *Biochem J.* **180,** 37 (1979).
4. R. M. Brooks and G. Di Chiro, *Med. Phys.* **14,** 903 (1987).
5. J. M. Gomori, R. I. Grossman, C. Yu-Ip, and T. Asakura, *J. Comput. Assist. Tomogr.* **11,** 684 (1987).

6. L. A. HAYMAN, J. J. FORD, K. H. TABER, A. SALEEM, M. E. ROUND, AND R. N. BRYAN, *Radiology* **168,** 489 (1988).
7. R. M. WEISSKOFF, S. R. KIIHNE, M. S. COHEN, AND K. R. THULBORN, *in* "Book of Abstracts, 10th Annual Meeting of the Society of Magnetic Resonance in Medicine, 1991," p. 307.
8. G. A. WRIGHT, B. S. HU, AND A. M. MACOVSKI, *J. Magn. Reson. Imaging* **1,** 275 (1991).
9. S. OGAWA, T. LEE, A. S. NAYAK, AND P. GLYNN, *Magn. Reson. Med.* **14,** 68 (1990).
10. S. OGAWA AND T. LEE, *Magn. Reson. Med.* **16,** 9 (1990).
11. B. E. HOPPEL, R. M. WEISSKOFF, K. R. THULBORN, J. MOORE, AND B. R. ROSEN, *in* "Book of Abstracts, 10th Annual Meeting of the Society of Magnetic Resonance in Medicine, 1991," p. 308.
12. A. VILLRINGER, B. R. ROSEN, J. W. BELLIVEAU, J. L. ACKERMAN, R. B. LAUFFER, R. B. BUXTON, Y. CHAO, V. J. WEEDEEN, AND T. J. BRADY, *Magn. Reson. Med.* **6,** 164 (1988).
13. C. R. FISEL, J. L. ACKERMAN, R. B. BUXTON, L. GARRIDO, J. W. BELLIVEAU, B. R. ROSEN, AND T. J. BRADY, *Magn. Reson. Med.* **17,** 336 (1991).
14. P. HARDY AND R. M. HENKELMAN, *Magn. Reson. Med.* **17,** 348 (1991).
15. S. MAJUMDAR, *Magn. Reson. Med.* **22,** 101 (1991).
16. R. TURNER, D. LE BIHAN, C. T. MOONEN, D. DESPRES, AND J. FRANK, *Magn. Reson. Med.* **22,** 159 (1991).
17. R. TURNER, A. BIZZI, D. DESPRES, J. ALGER, AND G. DI CHIRO, *in* "Book of Abstracts, 10th Annual Meeting of the Society of Magnetic Resonance in Medicine, 1991," p. 1032.
18. T. J. BRADY, *in* "Book of Abstracts, 10th Annual Meeting of the Society of Magnetic Resonance in Medicine, 1991," p. 2.
19. P. A. BANDETTINI, E. C. WONG, R. S. TIKOFSKY, R. S. HINKS, AND J. S. HYDE, *J. Magn. Reson. Imaging,* 1992, (2P), p. 76. [Abstract]
20. K. H. PRIBRAM, "Brain and Perception: Holonomy and Structure in Figural Processing," Erlbaum, Hillsdale, New Jersey, 1991.
21. A. JESMANOWICZ, E. C. WONG, J. C. WU, AND J. S. HYDE, *in* "Book of Abstracts, 10th Annual Meeting of the Society of Magnetic Resonance in Medicine, 1991," p. 740.
22. P. T. FOX AND M. E. RAICHLE, *Proc. Natl. Acad. Sci. USA* **83,** 1140 (1986).
23. G. PAWLIK, A. RACKL, AND R. J. BING, *Brain Res.* **208,** 35 (1981).
24. P. T. FOX, M. A. MINTUN, M. E. RAICHLE, F. M. MIEZIN, J. M. ALLMAN, AND D. C. VAN ESSEN, *Nature* **323,** 806 (1986).
25. D. W. JOHNSON, W. A. STRINGER, M. P. MARKS, W. F. GOOD, AND D. GUR, *AJNR,* **12,** 201 (1991).
26. W. W. ORRISON, L. E. DAVIS, G. W. SULLIVAN, F. A. METTLIER, AND E. R. FLYNN, *AJNR,* **11,** 713 (1990).
27. E. J. POTCHEN AND M. J. POTCHEN, *Invest. Radiol.* **26,** 258 (1991).
28. J. W. BELLIVEAU, D. N. KENNEDY, R. C. MCKINSTRY, B. R. BUCHBINDER, R. M. WEISSKOFF, M. S. COHEN, J. M. VEVEA, T. J. BRADY, AND B. R. ROSEN, *Science* **254,** 716 (1991).